Geochemistry Geophysics Geosystems G3
AN ELECTRONIC JOURNAL OF THE EARTH SCIENCES
Published by AGU and the Geochemical Society

Technical Brief
Volume 9, Number 3
6 March 2008
Q03005, doi:10.1029/2007GC001850
ISSN: 1525-2027

Directional median filtering for regional-residual separation of bathymetry

Seung-Sep Kim and Paul Wessel

Department of Geology and Geophysics, School of Ocean and Earth Science and Technology, University of Hawaii, 1680 East-West Road, Honolulu, HI 96822, USA (seungsep@hawaii.edu)

[1] We present a new spatial filter designed to separate short-length-scale bathymetric features from regional bathymetry. The directional median (DiM) filter divides a given filter circle into N "bow tie" sectors, allocates data points inside the filter circle to each sector based on their relative position within the circle, estimates a median for each sector, and returns the lowest of these N medians. This approach prevents DiM filtering from choosing the biased medians near the features on a sloping regional trend, which is a serious artifact of standard median filtering. As the bathymetry comprises diverse length-scale features, the separated results vary with the choice of filter width. Such variations are spatially distributed. Using a finite range of filter widths, we evaluate the spatial distribution of variations in the DiM-based separation by estimating their median absolute deviation (MAD) at each data point. The distribution of MAD values is indicative of uncertainties inherent in the separation. We demonstrate the effectiveness of DiM filtering with both synthetic and actual bathymetric data.

Components: 5450 words, 9 figures.

Keywords: regional-residual separation; bathymetry; spatial filtering; data analysis.

Index Terms: 0520 Computational Geophysics: Data analysis: algorithms and implementation; 3045 Marine Geology and Geophysics: Seafloor morphology, geology, and geophysics; 3252 Mathematical Geophysics: Spatial analysis (0500).

Received 10 October 2007; **Revised** 14 December 2007; **Accepted** 22 December 2007; **Published** 6 March 2008.

Kim, S.-S., and P. Wessel (2008), Directional median filtering for regional-residual separation of bathymetry, *Geochem. Geophys. Geosyst.*, *9*, Q03005, doi:10.1029/2007GC001850.

1. Introduction

[2] Regional-residual separation is a data processing task designed to extract a component of interest from the observations [*Telford et al.*, 1986]. For example, in geopotential studies the long-wavelength effects due to deep-seated structures need to be removed because they obscure the short-wavelength features in which we are most often interested. This task is of great importance in geophysical problems dealing with bathymetric data. For instance, both modeling the subsidence of the oceanic crust and quantifying depth anomalies require regional bathymetry unperturbed by small-scale features such as seamounts and swells [*Parsons and Sclater*, 1977; *Levitt and Sandwell*, 1996; *McNutt et al.*, 1996; *Hillier and Watts*, 2005]. The shapes of swells are used to estimate volume fluxes of hot spot materials [*White*, 1993; *Van Ark and Lin*, 2004; *Vidal and Bonneville*, 2004] whereas those of seamounts constrain the surface loads that may cause flexural deformation of the lithosphere [*McNutt and Menard*, 1978; *Watts*, 1978; *Lambeck*, 1981; *Kruse et al.*, 1997; *Ali et al.*, 2003]. Although each bathymetric feature

is associated with specific geologic processes, some of those features are often superimposed. Thus the definition of regional depends on the features of interest. Furthermore, unprocessed bathymetry may hinder subsequent data processing [*Little et al.*, 1993] and lead to different modeling results [*Watts and ten Brink*, 1989; *Wessel*, 1993].

[3] Curiously, the regional-residual separation of bathymetry is often practiced in irreproducible ways and poorly documented in science literatures (if at all). In order to define regional bathymetry, for instance, *Menard* [1973] made "visual estimates of the average depth" from bathymetric maps and *Sclater et al.* [1975] "drew smoothed lines" through bathymetric profiles. Since then, a few attempts have been made to develop robust separation methods [e.g., *Smith*, 1990; *Wessel*, 1998; *Hillier and Watts*, 2004; *Adam et al.*, 2005]. In this study, we will present a new spatial filter that isolates short-length-scale bathymetric features (e.g., seamounts) efficaciously while leaving the background bathymetry relatively unaltered. The effectiveness of our new filtering method may be maximized in regions where the separation of length scales of bathymetric features is distinct (e.g., seamounts sitting on a swell). As implied above, however, the variations in length scales are quite substantial and hence using one length scale (i.e., filter width) to process the bathymetry in a study area can be questionable [e.g., *Smith*, 1990]. In this respect, the main advance of our study is the evaluation of uncertainties inherent in the separation. In addition to removing unwanted parts from bathymetric data [e.g., *White and Hodges*, 2005; *White et al.*, 2006], our method may have other uses such as isolating pockmarks in sedimentary settings or volcanic cones in subaerial settings.

2. Methodology

[4] Bathymetric data reflect the sum of many different geologic processes exhibiting diverse length scales. As there is not enough physical information to disassemble the data according to each process, we constitute a residual bathymetry with bathymetric features of interest [*Telford et al.*, 1986]. For example, if swells are of interest, the other bathymetric features (e.g., broad subsidence of the oceanic crust and all seamounts) need to be removed [*Adam et al.*, 2005]. Because bathymetric features are hierarchical in length scales (i.e., small-scale features sit on top of broader features), it is easier to accomplish the separation by removing smaller features first [*Wessel*, 1998; *Hillier and Watts*, 2004]. For the separation of swells, one can remove seamounts first and then isolate swells from the rest of bathymetry [*Hillier and Watts*, 2004; *Adam et al.*, 2005]. In this way, the residual bathymetry comprises the separated features of interest and can be used as the observed data for any subsequent modeling. The definition of the residual bathymetry, therefore, is not an absolute concept but is tailored to each scientific problem; typically the residual seeks to isolate short-length-scale features.

[5] Traditional methods used for the removal of short-length-scale features include manual inspection [*Menard*, 1973; *Sclater et al.*, 1975; *Nettleton*, 1976] and a variety of low-pass [*Mesko*, 1965; *Telford et al.*, 1986], convolution [*Watts and Daly*, 1981; *Cazenave and Dominh*, 1987], and nonlinear filters [*Smith*, 1990; *Levitt and Sandwell*, 1996; *McNutt et al.*, 1996]. Both characteristics and shortcomings of these methods have been well documented by other researchers [e.g., *Wessel*, 1998; *Hillier and Watts*, 2004; *Adam et al.*, 2005]. For this study, we briefly demonstrate the performance of the spatial Gaussian, median, and mode filters using the synthetic data. In Figure 1a, a cone of diameter 6 and height 3 in arbitrary units is superimposed on a sloping plane. Therefore the expected regional (or best filtered) result is the original sloping plane. The tested filters, however, are unable to reproduce the expected plane and result in biased regional trends instead (Figures 1b, 1c, and 1d). To perform regional-residual separation effectively the proposed study seeks to remedy this problem by using the least biased median estimates in the vicinity of short-length-scale features, as described below.

[6] The median is a statistic of a data distribution that is relatively insensitive to outliers [e.g., *Davis*, 1986] and less fluctuating than the mode [e.g., *Wessel*, 1998]. Application of the median has been effective in various fields of data analysis [e.g., *Rousseeuw and Leroy*, 1987; *Wessel*, 1998; *Bovik*, 2005; *White and Hodges*, 2005]. As for regional-residual separation, the median can represent a regional depth when the number of data points from outliers (e.g., the cone) is less than half of the entire data points inside a filter circle [*Wessel*, 1998]. As the distribution of data points is skewed toward the regional, the median is obtained from the regional depths (e.g., Figure 2b). However, such asymmetry is disturbed when the regional exhibits a sloping trend, because data points from

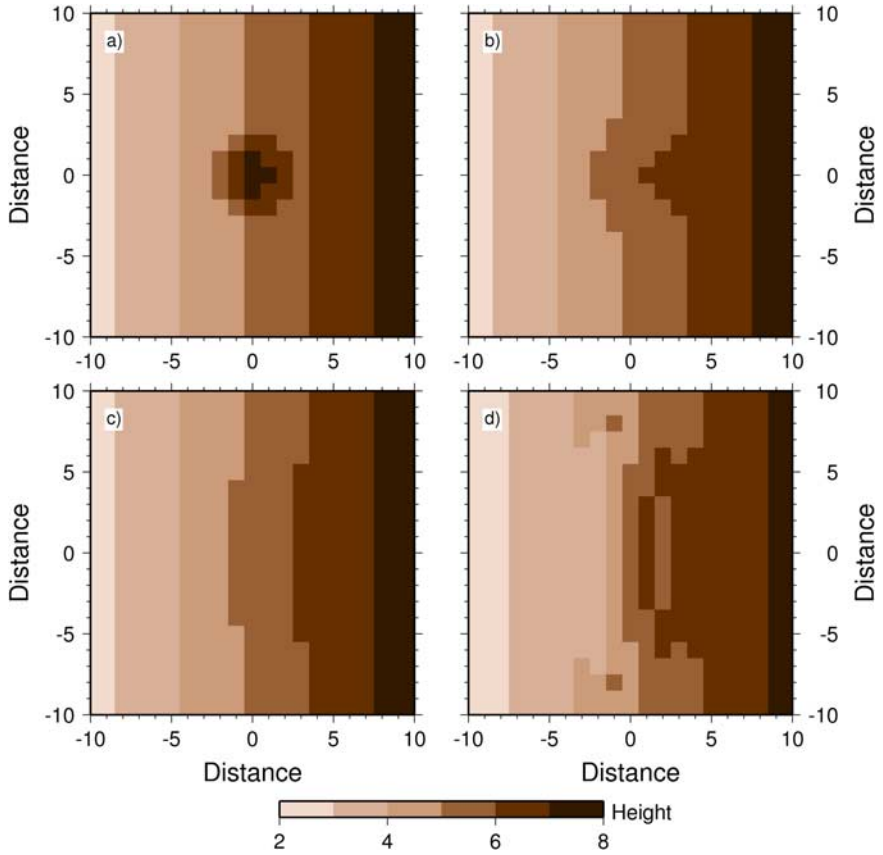

Figure 1. Comparison of spatial Gaussian, median, and mode filters on the synthetic data composed of a cone on a sloping plane. (a) Original synthetic data. (b) Gaussian-filtered result. (c) Median-filtered result. (d) Mode-filtered result. The filter width (i.e., the diameter of the filter circle), $w = 12$, twice as large as the width of the cone was used for each filtering. The units of height and distance are arbitrary.

the regional trend can vary significantly in depth (e.g., Figure 2d). Thus, as demonstrated in Figures 1c and 2d, median estimates obtained around any short-length-scale features sitting on a slope will be pulled up (i.e., become shallower than the expected trend). This shallowing of the median-filtered results is thus to be anticipated in regions where the superposition of short-length-scale features and slopes is apparent in the bathymetry [*Wessel*, 1998; *Adam et al.*, 2005].

[7] In this study, we mitigate the artifacts of median filtering due to slopes by using depth values from the sector most perpendicular to the local slope (i.e., the sector generally aligned with the strike of the slope). Because the regional trend in this direction is essentially flat with data points tightly clustered as in Figure 2b, the median is again insensitive to the outliers (e.g., the cone).

[8] To locate this particular sector, we divide the filter circle into N equal-sized "bow tie" sectors (see Figure 3a). Each data point is allocated to one of the N sectors on the basis of its relative position within the filter circle. Then, we obtain medians from each of these subsets, yielding N distinct answers. Because of the slope, the medians are pulled up by different amounts depending on sector orientation (see histograms in Figure 3). In the sector perpendicular to the slope, we find the least biased median as the data values are tightly grouped (sector 5 in Figure 3). This median is the lowest value among the N medians. Therefore searching the sector perpendicular to the local slope is equivalent to choosing the lowest median.

[9] As our filtering operation is designed to return medians from data elongated in a certain direction, we call the technique directional median (DiM) filtering. The technique has been programmed in C as a separate tool based on the spatial median filter routine in grdfilter of GMT [*Wessel and Smith*, 1998]; the source code is available upon request.

[10] Because bathymetric data are typically organized in a rectangular grid, the numbers of data points in each sector are rarely the same. With smaller N, one is unlikely to have a sector well

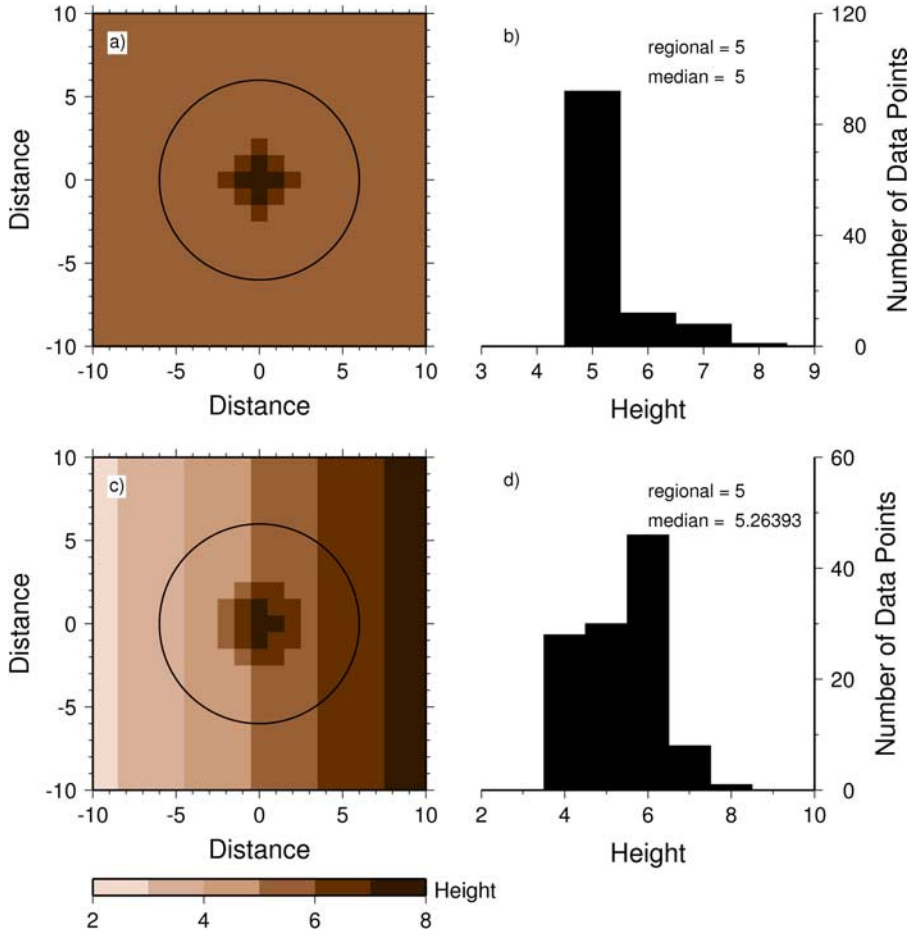

Figure 2. Illustration of median filtering artifacts due to slopes. (a, c) Snapshots of median filtering on flat (Figure 2a) and sloping (Figure 2c) planes. The cone from Figure 1a is placed on a flat plane. The circle indicates the location of the filter circle (w = 12). (b, d) Histograms of data points inside the filter circle located at (0,0) as shown in Figures 2a and 2c, respectively.

aligned with the strike of the sloping plane because there are too few sectors to represent all strikes. With larger N, too few data points are given to each sector so that each median may become statistically insignificant. A finer data grid spacing may obviate the latter problem but will also decrease computational efficiency. Therefore one must make compromises between having enough data points per sector and enough sectors to sense the direction most perpendicular to the slope. On the basis of considerable experimentation, we use N = 8 bow tie sectors for this study (Figure 3a). In Figure 3b, this new filtering method restored the true sloping plane by fully removing the cone.

[11] As for other spatial filters, DiM filtering results also rely on the chosen filter widths. *Wessel* [1998] suggested a quantified approach, called optimal robust separation (ORS), to finding filter widths that are optimal for removing small features. Using DiM filtering, we employ the ORS technique on synthetic data generated by superposing a Gaussian feature of diameter 30 km and height 5 km on top of a truncated cone of diameter 300 km and height 2 km (Figure 4a). To simulate a seamount formed on a swell, the truncated cone was first smoothed by Gaussian filtering (w = 50 km).

[12] The ORS method performs regional-residual separation for a range of filter widths. As the filter width increases, the Gaussian feature separated in the residual will initially grow (Figure 4d). This growth is quantified by the volume of the residual above a small positive contour level. As numerical noise causes meandering of the zero contour, a small positive level needs to be chosen (e.g., 50 m for Figure 4). The area of closed contours for this level also begins to grow (Figure 4c). However, the growth rates of these two measures are different, as compared in Figures 4c and 4d. The volume increases faster than the area because the contour line quickly reaches the base of the feature (Figure

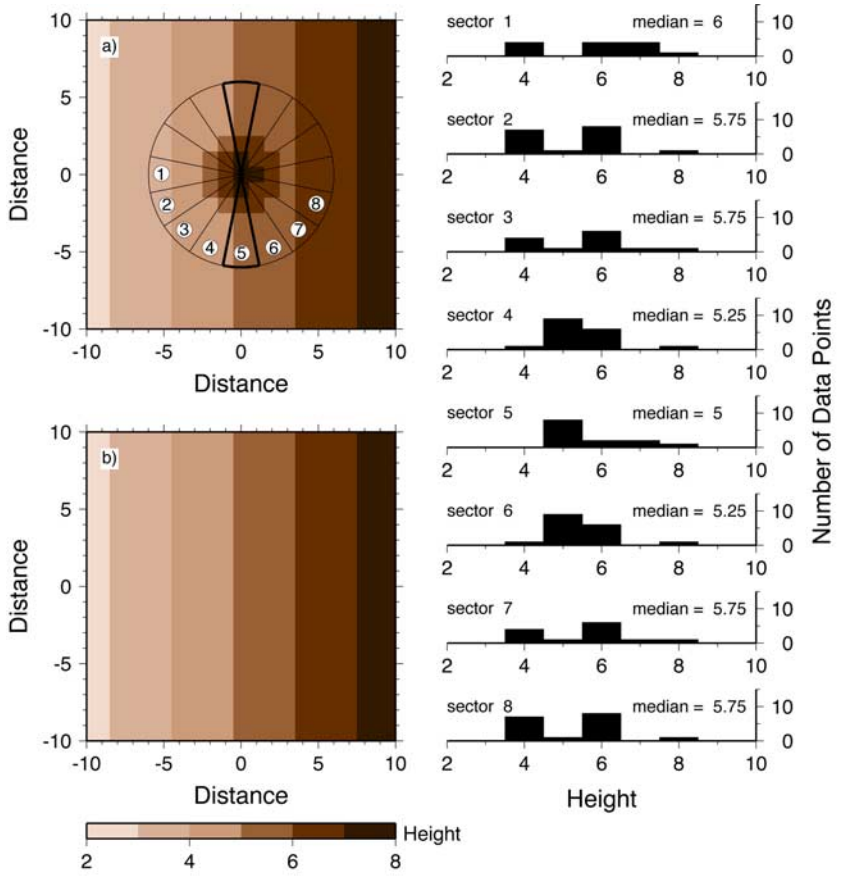

Figure 3. Directional median (DiM) filter. (a) Schematic diagram of DiM filter. DiM filtering divides its filter circle into eight "bow tie" sectors, computes the median value for each sector, and returns the lowest median estimate. The sector perpendicular to the sloping plane is in bold and numbered as 5. (right) Histograms of data points inside each sector are compared. Note that the median in sector 5 is the lowest value and represents the regional height. (b) DiM-filtered (w = 12) result from the synthetic data of Figure 1a.

4c). When the filter width becomes large enough to start removing the swell, the relative change in the area exceeds that of the volume (see gray contour areas in Figure 4c and dashed lines in Figure 4d). Thus the mean amplitude, defined as the ratio of the volume above a positive level in the residual to the area of its closed contour, is maximized when the removal of the feature is complete (Figure 4b). For effective DiM filtering of bathymetry, we choose a finite range of filter widths that produces amplitudes within 0.5% of the maximum mean amplitude (e.g., w = 45 ± 5 km for the synthetic data in Figure 4).

[13] As bathymetric features are spatially distributed with multiple length scales, a finite range of filter widths can be appropriate for DiM filtering to remove some features, but too short or too long to process the others in a study area. Consequently, the uncertainties of the separation are spatially distributed and need to be assessed in the space domain. We evaluate the spatial distribution of uncertainties in the regional-residual separation due to the choice of filter widths as follows:

[14] 1. For each filter width, w_i, a regional candidate, f_i (x, y), is determined by filtering the observed bathymetry, h(x, y). The widths w_i vary within the finite range of filter widths constrained by the ORS technique, as discussed above. For each step i, the filter width was incremented by 5 km in this study.

[15] 2. The final regional bathymetry, f_m(x, y), is obtained by computing the median of all regional candidates at each data point.

[16] 3. The median absolute deviation (MAD) values, σ^*(x, y), at each data point are then computed with respect to f_m(x, y) [*Rousseeuw and Leroy*, 1987]:

$$\sigma^*(x,y) = 1.482 \times \text{median}|f_i(x,y) - f_m(x,y)| \qquad (1)$$

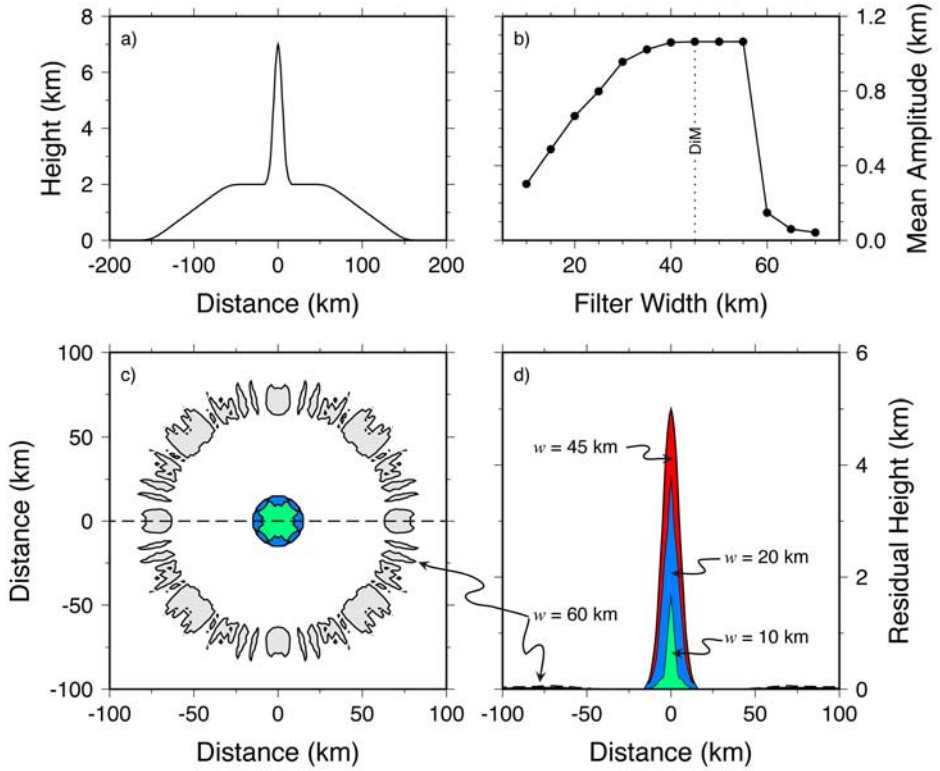

Figure 4. Demonstration of the optimal robust separation (ORS) method. (a) Synthetic data composed of a Gaussian feature and swell. This profile is made along the dashed line in Figure 4c over the synthetic data. (b) Mean amplitude variation computed by DiM filtering. (c) Changes in the area of contour lines (50 m) in the residual field. Each color indicates 50 m contours in the residual obtained by different filter widths. The red area is invisible as no significant increment is made when w = 45 km is applied. (d) Residual height variation over profile in Figure 4c. This shows the volume changes in the residual field indirectly. The volume increment (dashed line) for w = 60 km is negligible while the corresponding area, colored as gray in Figure 4c, has increased greatly, resulting in a sudden drop in the mean amplitude (Figure 4b).

The MAD values represent the amplitude of fluctuations in the DiM-filtered results at each data point with respect to the regional bathymetry; they measure the sensitivity of the separation to the choice of filter widths.

[17] 4. Finally, the residual bathymetry, $d(x, y)$, is obtained by subtracting the regional bathymetry from the observed data. The MAD values provide uncertainty bounds of the residual bathymetry, i.e.,

$$d(x,y) = h(x,y) - [f_m(x,y) \pm \sigma^*(x,y)]. \quad (2)$$

3. Results

[18] We demonstrate the effectiveness of the DiM filtering method by separating the Cape Verde Islands from the Cape Verde swell (Figure 5a) [*Young and Hill*, 1986; *McNutt*, 1988; *Ali et al.*, 2003]. The expected separation requires the complete removal of the islands while leaving the background bathymetry, especially the shape of the swell, relatively unaltered. The errors associated with the DiM-based separation are measured by the accompanying MAD analysis. In addition, the standard median-based separation presented by *Ali et al.* [2003] is reproduced for comparison with our DiM-based solution.

[19] The ORS technique was first used to determine the filter widths for both the DiM- and median-based separations (Figure 5b). If no data exist beyond the area of interest, then the number of data points inside the filter circle would be decreasing as filtering approaches to the edges of the data domain. The filtered values near the edges, thus, can be biased due to lack of data points. In order to avoid such edge effects, the filtering domain was extended in both directions by half the maximum filter radius. A secondary spatial median filtering (with w = 50 km) was applied to smooth the DiM-filtered data. To obtain the mean

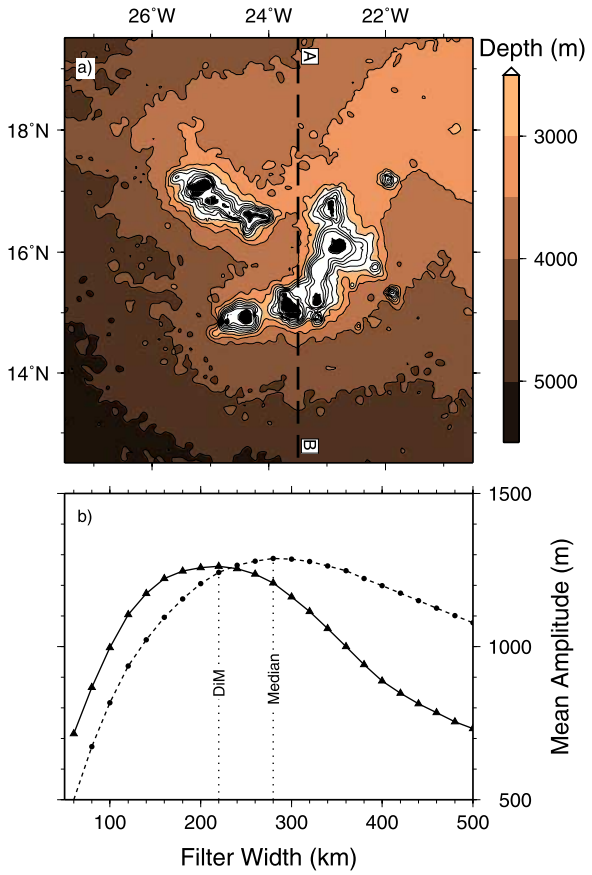

Figure 5. Bathymetry and mean amplitude variation of the Cape Verde Islands. (a) Predicted bathymetry (1 arc min grid spacing) from a blend of satellite-derived gravity and ship track data [*Smith and Sandwell*, 1997]. Following the study of *Ali et al.* [2003], the bathymetry and filtered results along profile AB are compared in Figure 7. Contour interval is 500 m. (b) Mean amplitude variation obtained by median (dashed line with circles) and DiM (solid line with triangles) filters. The best separation result is expected when the filter width maximizing the mean amplitude is used [*Wessel*, 1998].

amplitude for each filter width, the volume and area of the residual above 300 m were computed inside the original domain (Figure 5b). On the basis of the maximum mean amplitude, we chose w = 220 ± 20 km to carry out the DiM-based regional-residual separation as described above and w = 280 km for the standard median-based separation.

[20] The approximations to the Cape Verde swell made by median and DiM filtering are compared in Figure 6. As the overall shape of the swell is depicted by the bathymetry contours in Figure 5a, we can make a first-order assessment of the filtered results by examining how the contours of the regional bathymetry deviate from those of the original bathymetry (see white lines in Figure 6). This criterion satisfies the requirement we set earlier (i.e., relatively unaltered ambient data).

[21] The median-based swell with w = 280 km (Figure 6a) generally follows the bottom contours of the swell but introduces filtering artifacts due to the slopes in the vicinity of the islands. The amplitudes of such artifacts are significant along profile AB (see dashed line in Figure 7). To circumvent this problem, *Ali et al.* [2003] used w = 500 km for their best separation (Figure 6b) and substantiated their choice of filter width by showing the reduced amplitude of the artifacts along profile AB (see dotted line in Figure 7). We reproduced their approach by choosing the same profile of *Ali et al.* [2003]. However, the contours of the regional bathymetry in Figure 6b (w = 500 km) become much smoother than those of the original bathymetry, particularly for the eastern part of the swell.

[22] As for the DiM-based separation (w = 220 ± 20 km), the original contour lines are preserved relatively well (Figure 6c). The choice of the shorter filter widths is also supported by the profile in Figure 7. The spatial distribution of the MAD values in Figure 6d indicates the areas most sensitive to changes in the filter widths. Overall, the MAD values are less than 50 m for most areas but become larger beneath the islands. This uneven distribution implies that the multilength-scale nature of bathymetric features is the main error source in the separation and that by using a range of filter widths we may examine this contribution.

[23] In Figure 8, the DiM-based residual bathymetry is compared with the median-based residual (w = 500 km) used in the flexure study by *Ali et al.* [2003]. The equations describing any sophisticated flexure model make the common starting assumption that the load is placed on top of an initially flat elastic plate [*Watts*, 2001]. In order to use these equations properly, the residual bathymetry should go to zero away from the volcanic load; otherwise any significant topography would represent an artificial loading in the subsequent flexural modeling. In this point of view, the DiM-based residual shows the islands on a background of evenly distributed, near-zero values (Figure 8a). However, the median-based residual (Figure 8b) introduces additional long-wavelength contributions that are not associated with the islands themselves.

[24] As stated earlier, our main focus is on bathymetric features that exhibit positive departures

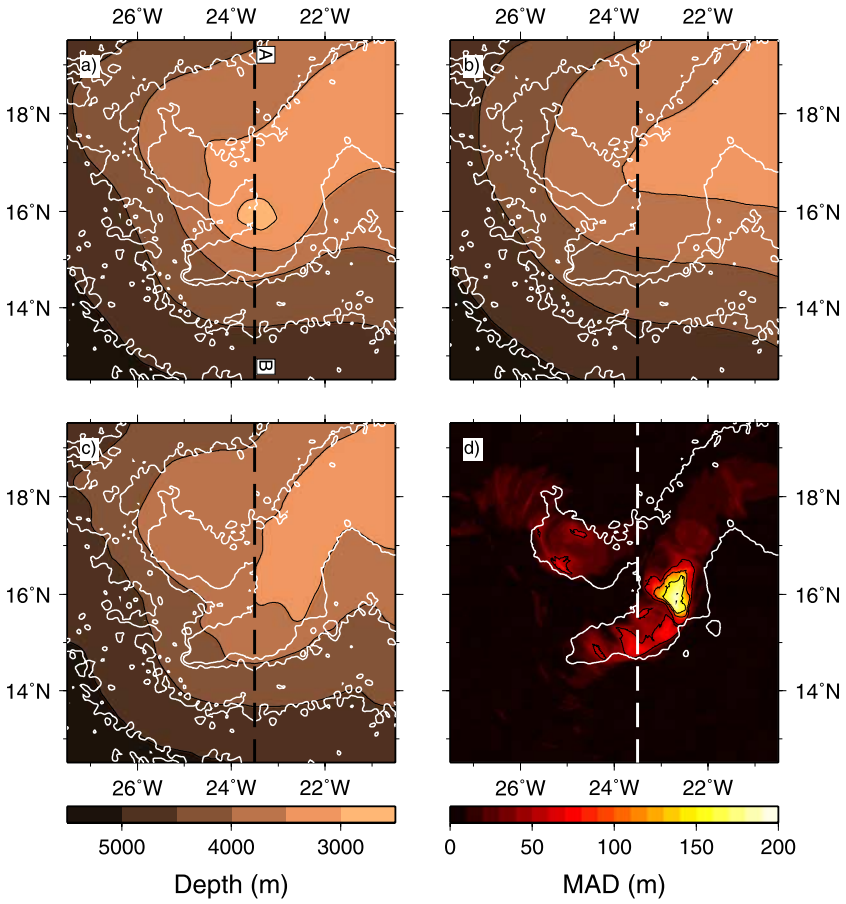

Figure 6. Cape Verde swell estimated by median and DiM filters. (a) The 280 km median filter result. (b) The 500 km median filter result as used in the study of *Ali et al.* [2003]. (c) DiM-filtered result (w = 220 ± 20 km). (d) Distribution of median absolute deviation (MAD) values from the DiM-filtered result in Figure 6c. The white solid lines in Figures 6a–6c are the contours of the original bathymetry, and those in Figure 6d are the 3500 m isobaths. Contour interval is 500 m. The filtered results along profile AB (dashed line) are compared in Figure 7.

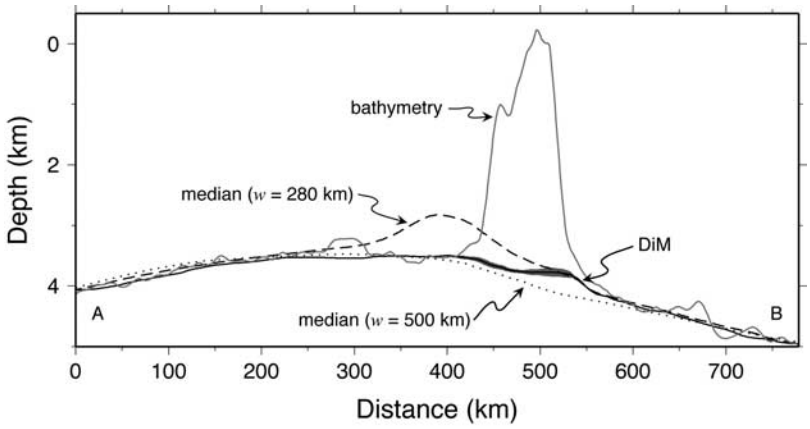

Figure 7. Comparison of the bathymetry, median, and DiM-filtered results along profile AB indicated in Figures 5a and 6. The gray line is the bathymetry, the dashed and dotted lines are the median-filtered results shown in Figures 6a and 6b, respectively, and the solid line is the DiM-filtered result (Figure 6c). The shaded region (most evident in the 500–550 km range) indicates the uncertainties of the DiM-based separation, based on the MAD analysis (Figure 6d).

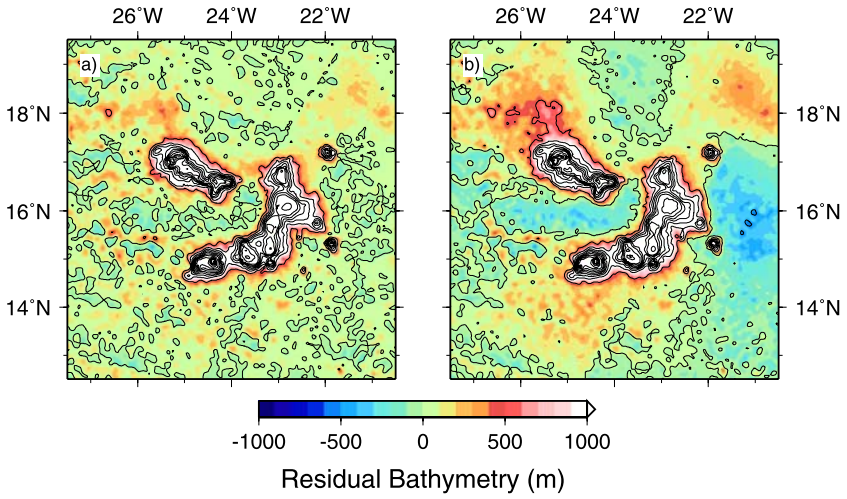

Figure 8. Comparison of residual bathymetry for the Cape Verde Islands. (a) DiM-based. (b) Median-based. Contour interval is 500 m.

from the background bathymetry, such as seamounts and swells. Thus our motivation for developing DiM filtering is to enhance the separation of such features. The usage of DiM filtering, however, is not limited to such convex features. As an example, we present the regional-residual separation of the Emperor Trough bathymetry (Figure 9a). Because regional bathymetry can be used to constrain depth anomalies [e.g., *Adam and Bonneville*, 2005; *Hillier and Watts*, 2005], the desired result is a regional bathymetry that excludes the trough. The DiM-filtered results are smoothed by a secondary median filtering (w = 50 km), as practiced earlier.

[25] When a filter width w = 100 km is applied, the median-based regional is pulled up while the DiM-based regional is pulled down (see dotted lines in Figure 9b). For DiM filtering, this width is too short as it allows the trough to pull down the regional significantly. For median filtering, the same filter width is large enough to regard the deep trough as outliers. However, we observe the shallowing of the regional due to the flanks of the trough and the slope. As the trough is juxtaposed with its flanks,

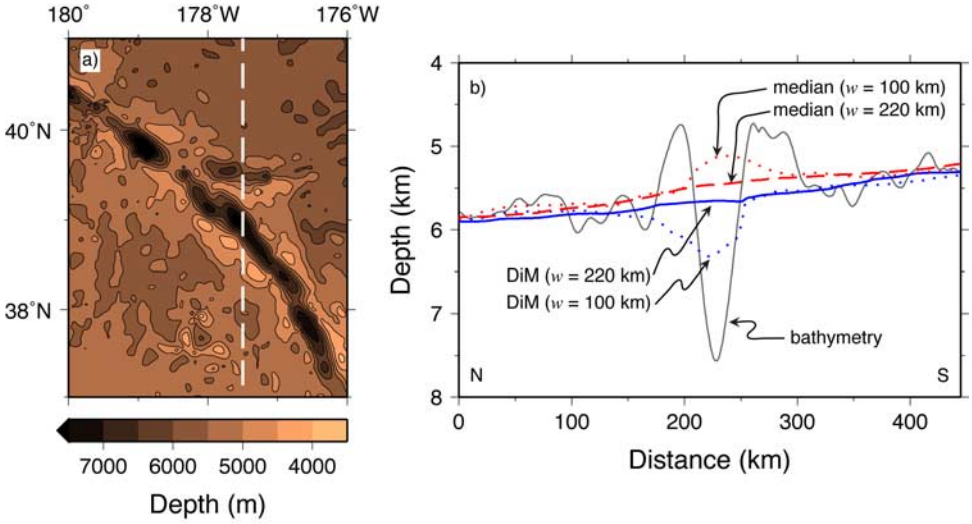

Figure 9. Comparison of median and DiM filtering at the Emperor Trough. (a) Predicted bathymetry (1 arc min grid spacing) from a blend of satellite-derived gravity and ship track data [*Smith and Sandwell*, 1997]. (b) Comparison of median- and DiM-filtered results along the dashed line in Figure 9a. The gray line is the bathymetry, and red and blue lines represent the median- and DiM-filtered results, respectively.

the total length scale of the trough and the flanks is larger than 100 km. With w = 220 km, the median-based regional still remains too shallow while the DiM-based regional is congruent with the general trend of the background bathymetry.

4. Discussion

[26] The DiM filtering technique provides an alternative way to separate short-length-scale features from what is considered the slowly varying regional background. Other applications of DiM filtering may include such tasks as separating pockmarks or mounds in sedimentary environments, volcanic cones in subaerial environments, and craters in extraterrestrial environments; the separated data can then be used for subsequent modeling. In flexure studies, for instance, the residual bathymetry (e.g., Figure 8a) defines the shape of the loading [*Minshull and Charvis*, 2001; *Watts*, 2001; *Ali et al.*, 2003]. As seamount groups may have many length scales, uncertainties in the separation due to selecting a finite range of filter widths seem inevitable (e.g., Figure 6d). However, the effect of such uncertainties on flexure modeling results has not been assessed.

[27] The ORS technique was demonstrated to determine the range of filter widths for the separation of the Cape Verde Islands from the underlying swell, where the difference between the length scales of the two different bathymetric features appears significant. In such cases, a range of filter widths that may be applicable to remove small features can be identified by the maximum mean amplitude. However, the different results shown in Figure 6 may imply that the ORS technique needs to be coupled with a more robust filtering method as both median and DiM filtering resulted in their own distinct maxima (Figure 5b). If the background bathymetry comprises more complex length scales, the mean amplitude computed by DiM filtering may either show no distinct maximum or be maximized at a false range of filter width (e.g., w = 500 km for 100 km length-scale features). Such behavior is anticipated at mid-ocean ridge areas and when the filtering domain is relatively large (e.g., Nazca plate) because both cases exhibit a continuum of length scales. A qualitative criterion to circumvent this problem is to set a range of filter widths that is at least twice the largest diameter of features to be removed. This may increase the chances of including more data points from the background bathymetry and hence obtaining a stable median inside the filter circle (e.g., Figure 2b). The separation result then can be assessed by the spatial distribution of MAD values. Another possible remedy is to use a variable range of filter widths based on the length scales of individual features (for one-dimensional (1-D) case, see *Hillier and Watts* [2004]).

[28] Finally, our method seeks the same end result as other techniques proposed recently, such as MiMIC [*Hillier and Watts*, 2004] and MiFil [*Adam et al.*, 2005]. A complete comparison between these disparate techniques is beyond the scope of this technical brief. Both MiMIC and MiFil have strengths and weaknesses. Here, we note in passing that MiMIC works along 1-D profiles and can only process 2-D grids using a mesh of profiles (ours works directly on 2-D grids) and that standard median filtering is one of the key steps in MiFil, a step we now have shown to be sensitive to sloping trends. We thus believe the DiM filtering method is a valuable alternative to these other techniques and is worth exploring further.

5. Conclusions

[29] We have developed a directional median (DiM) filtering method that (1) isolates short-length-scale features while leaving the background bathymetry relatively unchanged, (2) produces a separated result congruous with manual interpretation, and (3) allows users to evaluate the spatial distribution of uncertainties in the separation. This new spatial filter ameliorates the artifacts of spatial median filtering that occur when separating small-scale features from a sloping background. From case studies using synthetic and real bathymetric data, we have shown that DiM filtering produces a more reliable regional-residual separation than can be obtained with standard spatial median filtering. We conclude that the DiM filtering method is an efficient and effective tool for regional-residual separation of bathymetry and has the added benefit of providing uncertainty estimates.

Acknowledgments

[30] We thank F. Duennebier, J. Mahoney, G. Sharman, and A. Bonneville for their constructive review of an early version of this paper. Thorough comments from reviewers J. Goff and N. Mitchell and Editor J. Tarduno contributed to significant improvements over the original manuscript. We also appreciate J. Hillier for his thoughtful comments. This study was supported by National Science Foundation grant OCE-00-04498 and is SOEST contribution 7241.

References

Adam, C., and A. Bonneville (2005), Extent of the South Pacific Superswell, *J. Geophys. Res.*, *110*, B09408, doi:10.1029/2004JB003465.

Adam, C., V. Vidal, and A. Bonneville (2005), MiFil: A method to characterize seafloor swells with application to the south central Pacific, *Geochem. Geophys. Geosyst.*, *6*, Q01003, doi:10.1029/2004GC000814.

Ali, M. Y., A. B. Watts, and I. Hill (2003), A seismic reflection profile study of lithospheric flexure in the vicinity of the Cape Verde Islands, *J. Geophys. Res.*, *108*(B5), 2239, doi:10.1029/2002JB002155.

Bovik, A. (Ed.) (2005), *Handbook of Image and Video Processing*, 2nd ed., Elsevier, Burlington, Mass.

Cazenave, A., and K. Dominh (1987), Global relationship between oceanic geoid and seafloor depth: New results, *Geophys. Res. Lett.*, *14*, 1–4.

Davis, J. C. (1986), *Statistics and Data Analysis in Geology*, 2nd ed., John Wiley, New York.

Hillier, J. K., and A. B. Watts (2004), "Plate-like" subsidence of the East Pacific Rise–South Pacific superswell system, *J. Geophys. Res.*, *109*, B10102, doi:10.1029/2004JB003041.

Hillier, J. K., and A. B. Watts (2005), Relationship between depth and age in the North Pacific Ocean, *J. Geophys. Res.*, *110*, B02405, doi:10.1029/2004JB003406.

Kruse, S. E., Z. J. Liu, D. F. Naar, and R. A. Duncan (1997), Effective elastic thickness of the lithosphere along the Easter Seamount Chain, *J. Geophys. Res.*, *102*, 27,305–27,317.

Lambeck, K. (1981), Flexure of the oceanic lithosphere from island uplift, bathymetry, and geoid height observations: the Society Islands, *Geophys. J. R. Astron. Soc.*, *67*, 91–114.

Levitt, D. A., and D. T. Sandwell (1996), Modal depth anomalies from multibeam bathymetry: Is there a south Pacific superswell?, *Earth. Planet. Sci. Lett.*, *139*, 1–16.

Little, S. A., P. H. Carter, and D. K. Smith (1993), Wavelet analysis of a bathymetric profile reveals anomalous crust, *Geophys. Res. Lett.*, *20*, 1915–1918.

McNutt, M. K. (1988), Thermal and mechanical properties of the Cape Verde Rise, *J. Geophys. Res.*, *93*, 2784–2794.

McNutt, M. K., and H. W. Menard (1978), Lithospheric flexure and uplifted atolls, *J. Geophys. Res.*, *83*, 1206–1212.

McNutt, M. K., L. Sichoix, and A. Bonneville (1996), Modal depths from shipboard bathymetry: There IS a south Pacific superswell, *Geophys. Res. Lett.*, *23*, 3397–3400.

Menard, H. W. (1973), Depth anomalies and the bobbing motion of drifting islands, *J. Geophys. Res.*, *78*, 5128–5137.

Mesko, A. (1965), Some notes concerning the frequency analysis for gravity interpretation, *Geophys. Prospect.*, *13*, 475–488.

Minshull, T. A., and P. Charvis (2001), Ocean island densities and models of lithospheric flexure, *Geophys. J. Int.*, *145*, 731–739.

Nettleton, L. L. (1976), *Gravity and Magnetics in Oil Prospecting*, McGraw-Hill, New York.

Parsons, B., and J. G. Sclater (1977), An analysis of the variation of ocean floor bathymetry and heat flow with age, *J. Geophys. Res.*, *82*, 803–827.

Rousseeuw, P. J., and A. M. Leroy (1987), *Robust Regression and Outlier Detection*, 1st ed., John Wiley, New York.

Sclater, J. G., L. A. Lawver, and B. Parsons (1975), Comparison of long-wavelength residual elevation and free air gravity anomalies in the North Atlantic and possible implications for the thickness of the lithospheric plate, *J. Geophys. Res.*, *80*, 1031–1052.

Smith, W. H. F. (1990), Marine geophysical studies of seamounts in the Pacific Ocean basin, Ph.D. thesis, Columbia Univ., New York.

Smith, W. H. F., and D. T. Sandwell (1997), Global sea floor topography from satellite altimetry and ship depth soundings, *Science*, *277*, 1956–1962.

Telford, W. M., L. P. Geldart, R. E. Sheriff, and D. A. Keys (1986), *Applied Geophysics*, Cambridge Univ. Press, London.

Van Ark, E., and J. Lin (2004), Time variation in igneous volume flux of the Hawaii-Emperor hot spot seamount chain, *J. Geophys. Res.*, *109*, B11401, doi:10.1029/2003JB002949.

Vidal, V., and A. Bonneville (2004), Variations of the Hawaiian hot spot activity revealed by variations in the magma production rate, *J. Geophys. Res.*, *109*, B03104, doi:10.1029/2003JB002559.

Watts, A. B. (1978), An analysis of isostasy in the world's oceans: 1. Hawaiian-Emperor seamount chain, *J. Geophys. Res.*, *83*, 5989–6004.

Watts, A. B. (2001), *Isostasy and Flexure of the Lithosphere*, 1st ed., Cambridge Univ. Press, London.

Watts, A. B., and S. F. Daly (1981), Long-wavelength gravity and topography anomalies, *Annu. Rev. Earth Planet. Sci.*, *9*, 415–448.

Watts, A. B., and U. S. ten Brink (1989), Crustal structure, flexure, and subsidence history of the Hawaiian islands, *J. Geophys. Res.*, *94*, 10,473–10,500.

Wessel, P. (1993), A reexamination of the flexural deformation beneath the Hawaiian Islands, *J. Geophys. Res.*, *98*, 12,177–12,190.

Wessel, P. (1998), An empirical method for optimal robust regional-residual separation of geophysical data, *J. Math. Geol.*, *30*, 391–408.

Wessel, P., and W. H. F. Smith (1998), New, improved version of Generic Mapping Tools released, *Eos Trans., AGU*, *79*, 579.

White, L., and B. R. Hodges (2005), Filtering the signature of submerged large woody debris from bathymetry data, *J. Hydrol.*, *309*, 53–65.

White, L., B. R. Hodges, B. N. Austin, and T. D. Osting (2006), Identification of submerged large woody debris from single-beam echo soundings, *J. Hydroinf.*, *7*, 1–12.

White, R. S. (1993), Melt production rates in mantle plumes, *Philos. Trans. Phys. Sci. Eng.*, *342*, 137–153.

Young, R., and I. A. Hill (1986), An estimate of the effective elastic thickness of the Cape Verde Rise, *J. Geophys. Res.*, *91*, 4854–4867.